Nano Research

ISSN 1998-0124 CN 11-5974/O4
https://doi.org/10.26599/NR.2025.94907123

Research Article

Exploring potential for semiconductor to quantum anomalous Hall insulator transitions via substrate-induced structural modifications in Ti_3Se_4 monolayers

Zhipeng Song[1,§], Haixia Cheng[2,6,§], Yun Cao[1], Qi Zheng[1], Yurou Guan[2], Chen Liu[3], Jierui Huang[1], Li Huang[1], Jiaou Wang[3], Hui Guo[1], Guangchao Chen[1], Chengmin Shen[1], Shixuan Du[1,4,5], Hongliang Lu[1,5](✉), Wei Ji[2](✉), Xiao Lin[1,5](✉), Hong-Jun Gao[1,4,5]

[1] University of Chinese Academy of Sciences and Institute of Physics, Chinese Academy of Sciences, Beijing 100190, China

[2] Beijing Key Laboratory of Optoelectronic Functional Materials & Micro-Nano Devices, Department of Physics, Renmin University of China, Beijing 100872, China

[3] Institute of High Energy Physics, Chinese Academy of Sciences, Beijing 100049, China

[4] Songshan Lake Materials Laboratory, Dongguan, Guangdong 523808, China

[5] CAS Center for Excellence in Topological Quantum Computation, University of Chinese Academy of Sciences, Beijing 100190, China

[6] Material Digital R&D Center, China Iron & Steel Research Institute Group, Beijing 100081, China

Nano Res., **Just Accepted Manuscript** • https://doi.org/10.26599/NR.2025.94907123

https://www.sciopen.com/journal/1998-0124 on Nov. 8, 2024

TOC

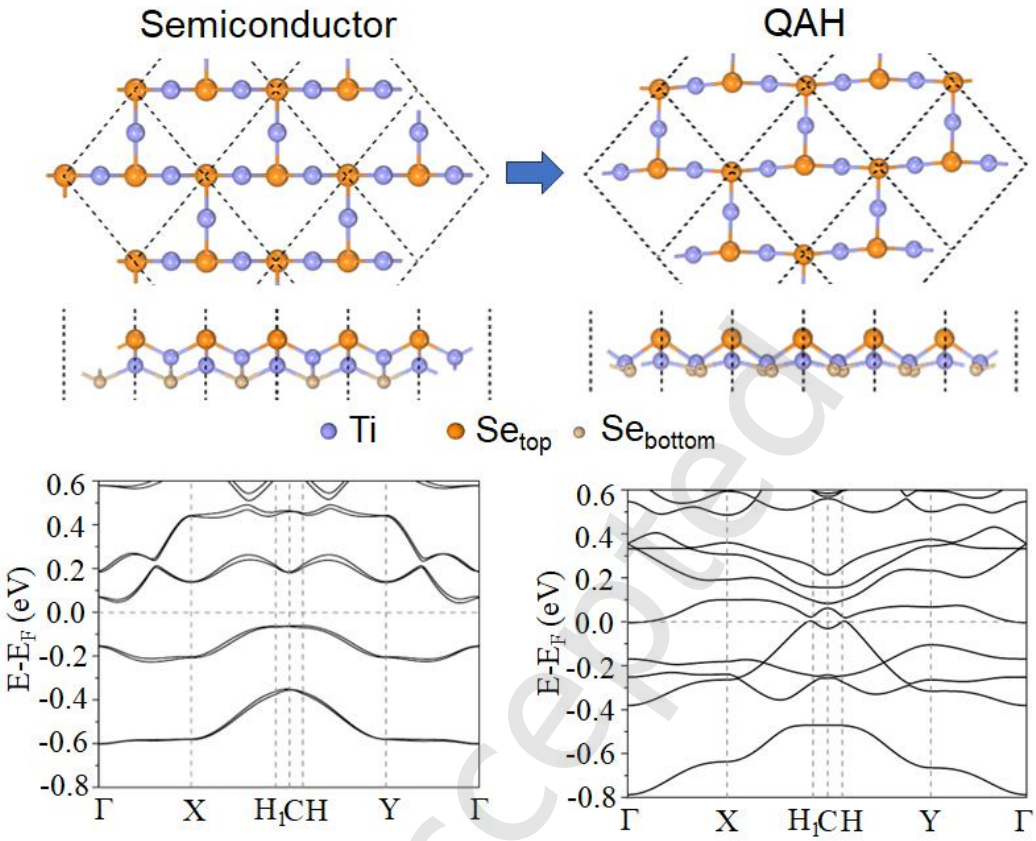

TOC

Semiconductor materials hold the potential to transform into QAH materials by adjusting their lattice structure.

Research Article

Exploring potential for semiconductor to quantum anomalous Hall insulator transitions via substrate-induced structural modifications in Ti_3Se_4 monolayers

Zhipeng Song[1,§], Haixia Cheng[2,6,§], Yun Cao[1], Qi Zheng[1], Yurou Guan[2], Chen Liu[3], Jierui Huang[1], Li Huang[1], Jiaou Wang[3], Hui Guo[1], Guangchao Chen[1], Chengmin Shen[1], Shixuan Du[1,4,5], Hongliang Lu[1,5] (✉), Wei Ji[2] (✉), Xiao Lin[1,5](✉) and Hong-Jun Gao[1,4,5]

[1]*University of Chinese Academy of Sciences and Institute of Physics, Chinese Academy of Sciences, Beijing 100190, China*

[2]*Beijing Key Laboratory of Optoelectronic Functional Materials & Micro-Nano Devices, Department of Physics, Renmin University of China, Beijing 100872, China*

[3]*Institute of High Energy Physics, Chinese Academy of Sciences, Beijing 100049, China*

[4]*Songshan Lake Materials Laboratory, Dongguan, Guangdong 523808, China*

[5]*CAS Center for Excellence in Topological Quantum Computation, University of Chinese Academy of Sciences, Beijing 100190, China*

[6]*Material Digital R&D Center, China Iron & Steel Research Institute Group, Beijing 100081, China*

Received: 27 August 2024; **Revised:** 17 October 2024; **Accepted:** 7 November 2024
Address correspondence to Hongliang Lu, luhl@ucas.ac.cn; Wei Ji, wji@ruc.edu.cn; Xiao Lin, xlin@ucas.ac.cn

Cite this article: *Nano Research*, **2025**, *18*, 94907123. https://doi.org/10.26599/NR.2025.94907123

ABSTRACT

The quantum anomalous Hall (QAH) effect in two-dimensional (2D) topological materials has attracted widespread attention due to its potential for dissipationless chiral edge transport without an external magnetic field, which is highly promising for low-power electronic applications. However, identifying materials that exhibit these properties remains particularly challenging, as only a limited number of such materials are known, raising the intriguing question of whether it is possible to induce the QAH effect in materials with ordinary

properties through structural modifications. In this work, we grow an unreported 2D titanium selenide (Ti_3Se_4) on a Cu(111) substrate using molecular beam epitaxy. Low-energy electron diffraction and scanning tunneling microscopy characterizations reveal a $\sqrt{7} \times \sqrt{7}$ brick-like structure. First-principles calculations and X-ray photoelectron spectroscopy measurements confirm its composition to be Ti_3Se_4. Our calculations further demonstrate that monolayer Ti_3Se_4, in its grown form on Cu(111), has the potential to host the QAH effect. Interestingly, when we examine its freestanding form, the monolayer transitions from a QAH insulator candidate into a conventional semiconductor, despite only minor differences in their atomic structures. This transition enlightens us that subtle lattice adjustments can induce a transition from semiconductor to QAH properties in freestanding Ti_3Se_4. This discovery provides a potential route to engineering practical materials that may exhibit the QAH effect.

KEYWORDS

quantum anomalous Hall effect, monolayer Ti_3Se_4, structural modifications, semiconductor, molecular beam epitaxy

1 Introduction

Topological insulators, distinguished by their topologically nontrivial band structures, have attracted significant research interest due to their unique physical properties and potential applications.[1-7] Among these, the quantum anomalous Hall (QAH) effect is particularly intriguing. It features topologically protected quantized Hall resistance and zero longitudinal resistance without an external magnetic field.[3, 8] Bulk topological insulators possess a band gap, while their surfaces exhibit gapless Dirac states protected by time-reversal symmetry. However, introducing ferromagnetic order through magnetic doping breaks this time-reversal symmetry, leading to the opening of a gap at the Dirac point in the surface states..[9] When the Fermi level falls within this exchange gap, a chiral edge mode emerges, giving rise to a topologically nontrivial electronic structure that manifests the QAH effect. [10-12] Materials exhibiting this effect hold significant potential for future low-power electronic applications.[8]

Despite their importance, materials that exhibit the QAH effect are exceedingly rare. The pioneering experimental observation of the QAH effect was in magnetically doped $(Bi,Sb)_2(Se,Te)_3$.[13-19] Finding intrinsic magnetic topological insulators is considered to be a crucial strategy for enhancing the critical temperature of the QAH effect. $MnBi_2Te_4$ is one such material, where the QAH effect is observed at 1.4 K without a magnetic field and 6.5 K with a magnetic field in a five-septuple-layer specimen.[11] The QAH effect was also observed in multilayer graphene[20-23] and AB-stacked $MoTe_2/WSe_2$ moiré heterobilayers.[24] However, the practical application of the QAH effect remains limited because of the instability of these materials in air and requirement for extremely low temperatures. Therefore, there is an urgent need to develop other methodologies to discover materials that exhibit the QAH effect that are suitable for practical applications.

In this work, we report a strategy to grow titanium selenides using molecular beam epitaxy (MBE), enabling fabrication of monolayer Ti_3Se_4, an unreported 2D material, on a Cu(111) substrate. Using a combination of scanning tunneling microscopy (STM), low-energy electron diffraction (LEED), X-ray photoelectron spectroscopy (XPS) and density functional theory (DFT) calculations, we characterized the brick-like atomic structure and the 3:4 composition of this material. Our first-principles calculations show that, while free-standing Ti_3Se_4 is a semiconductor, the Ti_3Se_4 monolayer in the form grown on the Cu(111) substrate has the

potential to exhibit QAH effect. Furthermore, although the QAH effect has been demonstrated in thin films or multi-layer materials, no studies have yet shown this effect in a monolayer where atoms are connected by covalent bonds.

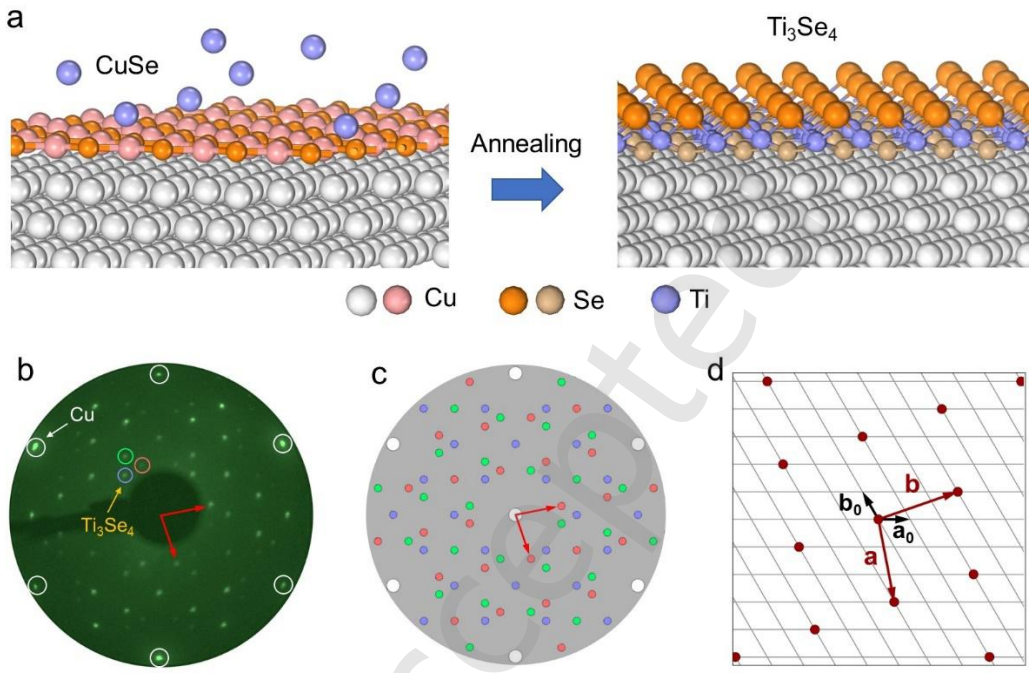

Fig. 1. The growth process and the structure of Ti_3Se_4. (a) Schematic illustrations of the growth process of Ti_3Se_4. (b) LEED pattern of Ti_3Se_4 formed on Cu(111) surface. The white circles indicate the diffraction spots of Cu(111) substrate and the additional diffraction spots are ascribed to the Ti_3Se_4. (c) Sketch of the diffraction spots shown in (b), which are generated by three domains as represented in different colors. (d) Schematic diagram of Ti_3Se_4 lattice in real space, corresponding to one set of the diffraction spots (the red spots) in (c). The dark red and black arrows show the lattice vectors of the monolayer Ti_3Se_4 and the Cu(111) substrate, respectively.

2 Experimental section and calculation

2.1 Sample preparation

Monolayer Ti_3Se_4 on Cu(111) substrate was grown in an ultra-high vacuum molecular beam epitaxy system with a base pressure lower than 5×10^{-10} mbar. The atomically clean

Cu(111) surface was obtained by cycles of argon-ion sputtering and annealing until clean surface was confirmed in STM images and sharp LEED patterns. Firstly, The high-purity Se (99.99%) was deposited to the clean Cu(111) substrate from Knudsen cell while the substrate was kept at 650 K to form the non-hole monolayer CuSe. Then Ti (99.9%) was deposited from electron-beam evaporators, and the substrate was kept at 650 K. Finally monolayer Ti_3Se_4 can be formed on the Cu(111) surface. After several experiments, we found that the effective way to fabricate this special 2D material Ti_3Se_4 is by using CuSe as a precursor. All the characterizations were done in ultra-high vacuum environment by using in-situ transfer technique. The LEED and STM characterizations were performed at a base pressure of $\sim 3 \times 10^{-10}$ mbar. LEED patterns were carried out with a commercial high-resolution instrument and the electron energy used in experiment was 66 eV. STM measurements were performed in the constant-current mode. In situ X-ray photoelectron spectroscopy measurements were performed at the Beijing Synchrotron Radiation Facility with a hemispherical energy analyzer.

2.2 Calculation details

Spin-polarized density functional theory (DFT) calculations were performed using the projector augmented wave method[25, 26] with the Perdew-Burke-Ernzerhof exchange correlation functional as implemented in the Vienna ab-initio simulation package.[27, 28] The density-dependent-dispersion-corrected PBE functional (PBE-dDsC) method was chosen for the van der Waals correction.[29-31] A kinetic energy cutoff of 500 eV for the plane-wave basis set was used. The Brillouin zone was sampled using a uniform Γ-centered 9×9×1 (15×15×1) Monkhorst-pack *k*-mesh for structural relaxations (electronic structure calculations) of monolayer Ti_3Se_4. Spin-orbit coupling (SOC) was considered in electronic structure calculations for monolayer Ti_3Se_4. The Ti_3Se_4/Cu(111) interface was modelled using a Ti_3Se_4 monolayer and five layers of the Cu(111) plane with two fixed bottom layers. A vacuum layer of ~15 Å was used to eliminate interactions between periodic layers. Fixing the lattice constant identical to the Cu substrate, atomic positions were relaxed until the residual force on each atom was less than 0.01 eV/Å. The edge states of monolayer Ti_3Se_4 were calculated by means of maximally localized Wannier functions implemented in the WANNIER 90 package.

3 Results and discussion

3.1 Structural characterization of monolayer Ti_3Se_4 grown on Cu(111) substrate

The ratio of Ti and Se in common titanium selenides is 1:2, and synthesizing a 3:4 phase is a challenging task due to the difficulty in controlling the ratio. Here, we used a monolayer CuSe/Cu(111) as a template to determine the amount of Se, and then only needed to control the amount of Ti to obtain Ti_3Se_4.The growth process is schematically shown in Fig. 1(a). High-purity Se was evaporated onto the Cu(111) surface to form monolayer CuSe.[32] The LEED pattern in Fig. S1(a) in the Supplemental Material shows hexagonal crystal structure and the STM image in Fig. S1(b) in the Supplemental Material shows atomically flat surface with 1D moiré pattern, which indicate the formation of CuSe on Cu(111) substrate.[32] Then Ti atoms were deposited on the CuSe/Cu(111) surface, which changed the LEED pattern to that shown in Fig. 1(b). The outer six diffraction spots highlighted by the white circles originate from the Cu(111) substrate with six-fold symmetry and the other distinct diffraction spots are assigned to the new material. For clarity, we sketched a simulated diffraction pattern of the sample in reciprocal space in Fig. 1(c), where each group of spots in different colors are derived from different domains and one group of the reciprocal vectors of such spots are depicted by the red arrows. The lattice of this 2D material in real space is schematically shown in Fig. 1(d), which is a $\sqrt{7} \times \sqrt{7}$ structure with respect to the Cu(111) substrate.

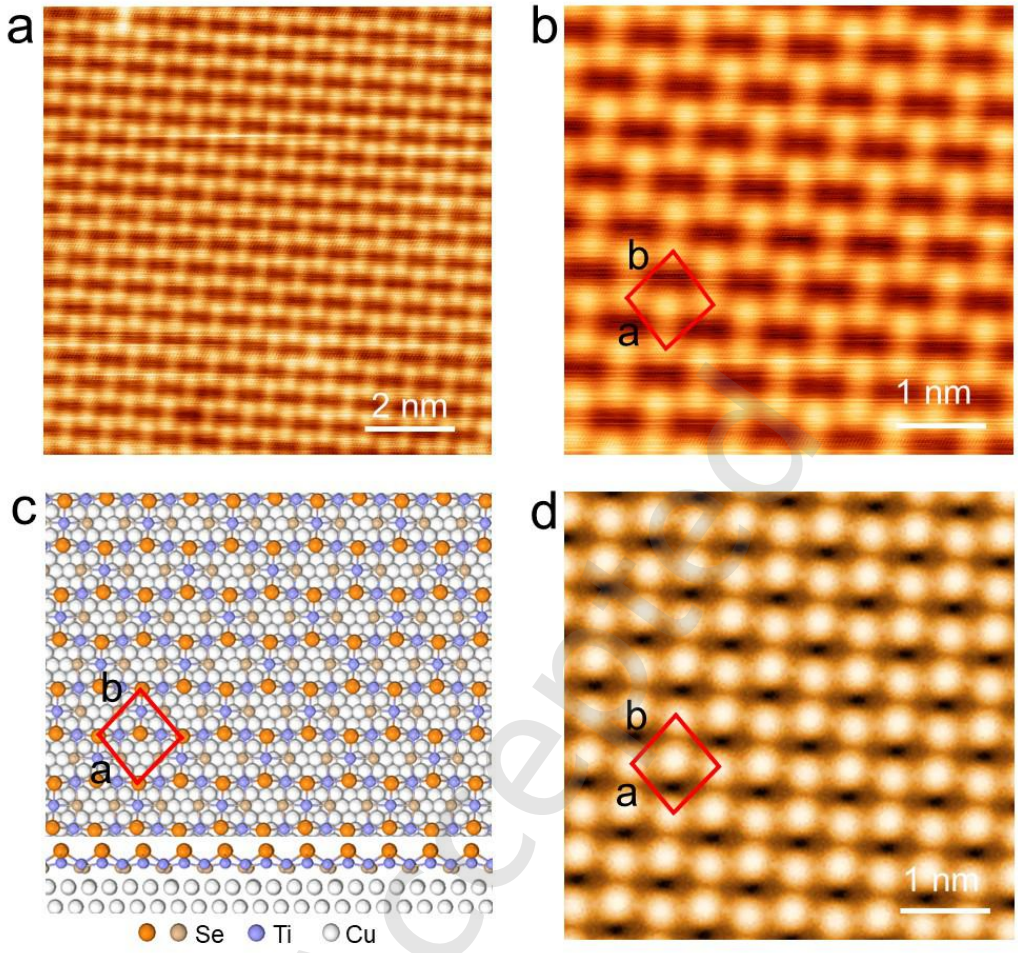

Figure 2. STM images and atomic configuration of monolayer Ti_3Se_4. (a) Large-scale STM image of Ti_3Se_4. (b) High-resolution STM image of monolayer Ti_3Se_4 (V_S = -0.7 V, I_t = 50 pA, T=4.5 k). (c) Top and side view of the atomic model of monolayer Ti_3Se_4 on Cu(111) substrate optimized by DFT calculation. (d) STM simulation of monolayer Ti_3Se_4 on Cu(111) substrate with V_S = -0.7 V.

Figure 2(a) presents a medium-scale STM image of Ti_3Se_4, while Fig. 2(b) displays a high-resolution STM image of this new 2D material, which exhibits a brick-like morphology. The primitive cell of crystal lattice is marked by a red rhombus, which shows an angle of approximately 100° between vectors *a* and *b*. The lattice constants of this primitive cell are about a=6.95 Å, b=7.08 Å. Figure S2(a) in the Supplemental Material shows a representative large-scale STM image, while Fig. S2(b) shows the morphology covering an edge of this material on Cu(111), showing that its height of approximately 0.47 nm (see Fig.S2(c)).

3.2 Structural confirmation of monolayer Ti_3Se_4

To confirm the structure of this 2D material, we constructed an atomic model of monolayer titanium selenide with a chemical formula of Ti_3Se_4 according to the experimentally obtained lattice constants. The optimized atomic structure of Ti_3Se_4/Cu(111) is shown in Fig. 2(c), in which the primitive cell was marked by a red rhombus. We compared experimental and simulated STM images, both acquired at a bias voltage of -0.7 V. These images are highly consistent in terms of surface morphology and lattice constants (see Figs. 2(b) and 2(d)). This consistency strongly supports that the experimentally fabricated 2D monolayer is indeed Ti_3Se_4, as depicted in Fig. 2(c). Further characterization of monolayer Ti_3Se_4 revealed that its STM morphology image varies under different biases. As shown in Fig. S3(a)-(c) in the Supplemental Material, the STM images show a brick-like morphology when the absolute bias value (|V|) exceeds 0.4 V, whereas a rectangular morphology is observed when the absolute bias value is below 0.4 V. The corresponding STM simulation images, presented in Fig. S3(d)-(f), are in good agreement with the experimental results. To verify the actual surface structure, we conducted atomic force microscopy (AFM) characterization. The results, shown in Fig. S4 in the Supplemental Material, are well consistent with the LEED pattern, indicating that the brick-like morphology is the inherent structure of monolayer Ti_3Se_4.

High-resolution XPS measurements were subsequently conducted to further verify the chemical composition of the sample. Figure S5(a) in the Supplemental Material shows the Ti 2p photoelectron spectrum which reflects two chemical states of the titanium. The two blue peaks are located at 454.3 eV and 460.4 eV, while the other two red peaks are located at 455.9 eV and 461.8 eV, respectively. Clearly, the valence state of titanium here is inconsistent with tetravalent titanium.[33, 34] If we compare the peaks of Ti $2p_{3/2}$ (454.3 eV and 455.9 eV) with the standard XPS spectra,[35] we find the oxidation states of Ti in this material are +2 and +3. The Se $3d_{3/2}$ and $3d_{5/2}$ peaks are located at 55.1 eV and 54.2 eV, respectively, as shown in Fig. S5(b) in the Supplemental Material, indicating the chemical state of Se^{2-} [35]. Therefore, the XPS measurement corroborate that this new 2D material is Ti_3Se_4.

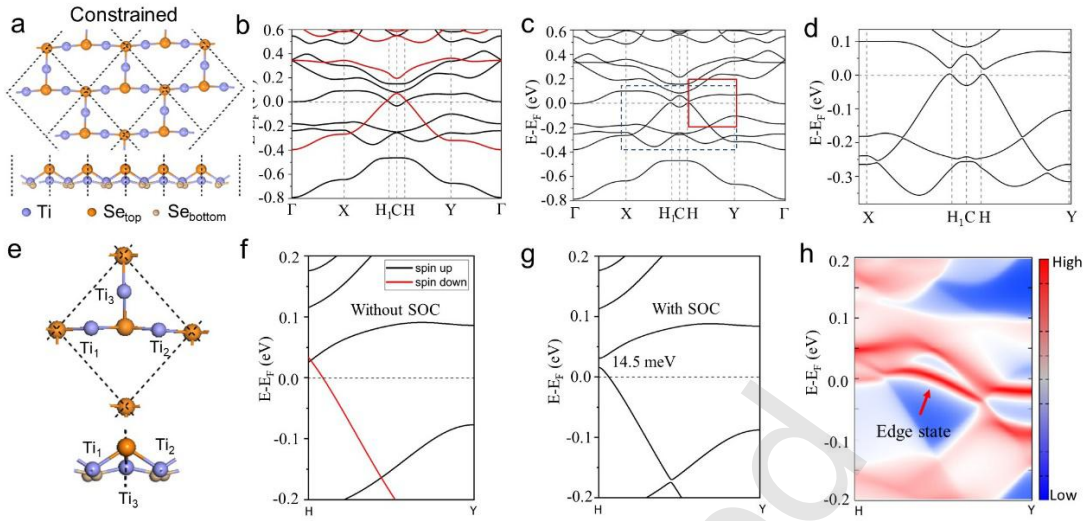

Figure 3. Calculated band structures of the constrained Ti_3Se_4. (a) The atomic model of the constrained Ti_3Se_4 by Cu(111) substrate. In the top panel, the bottom Se atoms are not depicted. (b, c) Calculated band structures of constrained Ti_3Se_4 without and with SOC, respectively. (d) Zoom-in band structures in the blue dashed rectangle in (c), showing an obvious SOC-induced energy gap near the Fermi level. (e) The primary source of magnetic moment in constrained monolayer Ti_3Se_4 arises from Ti atoms. (f, g) The band structures of constrained Ti_3Se_4 along the H-Y direction without and with SOC, respectively. (g) corresponds to the red rectangle in (c). (h) Edge state of the constrained Ti_3Se_4 denoted by the red arrow.

3.3 Band structures of the monolayer Ti_3Se_4

We next examined the potential applications of the as-fabricated Ti_3Se_4 in electronic devices by calculating its band structures using the Ti_3Se_4 monolayer structure directly detached from the fully relaxed Ti_3Se_4/Cu(111) interface (Figs. 2(c) and 3(a)). This model excluded the influence of the substrate, standing out the intrinsic electronic properties of the Ti_3Se_4 monolayer. Figure 3(b) shows the calculated band structures of the brick-like Ti_3Se_4 monolayer without SOC. The black and red curves represent the electronic bands with spin-up and -down components, respectively, revealing that the spin-up and spin-down bands cross near the Fermi level, close to points H_1 and H in the first Brillouin zone. Including SOC in the calculations results in energy gaps at the crossing points of these two bands, leading to band inversion as shown in Figs. 3(c) and 3(d). Figure 3(e) highlights the primary source of

magnetic moment in this constrained monolayer Ti_3Se_4 arising from Ti atoms. For clarity, magnified band structures of Ti_3Se_4 along the H-Y direction, both without and with SOC, are presented in Figs. 3(f) and 3(g), respectively. A gap of 14.5 meV is clearly identified above the Fermi level, close to the H point. Remarkably, this material exhibits a large magnetic moment (2.13 μ_B/cell) primarily resulted from the titanium atoms, as shown in Fig. 3(e). Considering the gap opening after SOC and the appearance of the large magnetic moment, we anticipate that this brick-like monolayer Ti_3Se_4 is a topological material capable of exhibiting the QAH effect. To further verify the QAH effect, we calculated the edge state of the brick-like Ti_3Se_4 monolayer. Figure 3(h) shows a detailed band structure diagram, clearly highlighting the edge state marked by the red arrow. The presence of the edge state, in addition to the SOC-induced gap, confirms that this monolayer satisfies the criteria of exhibiting the QAH effect.

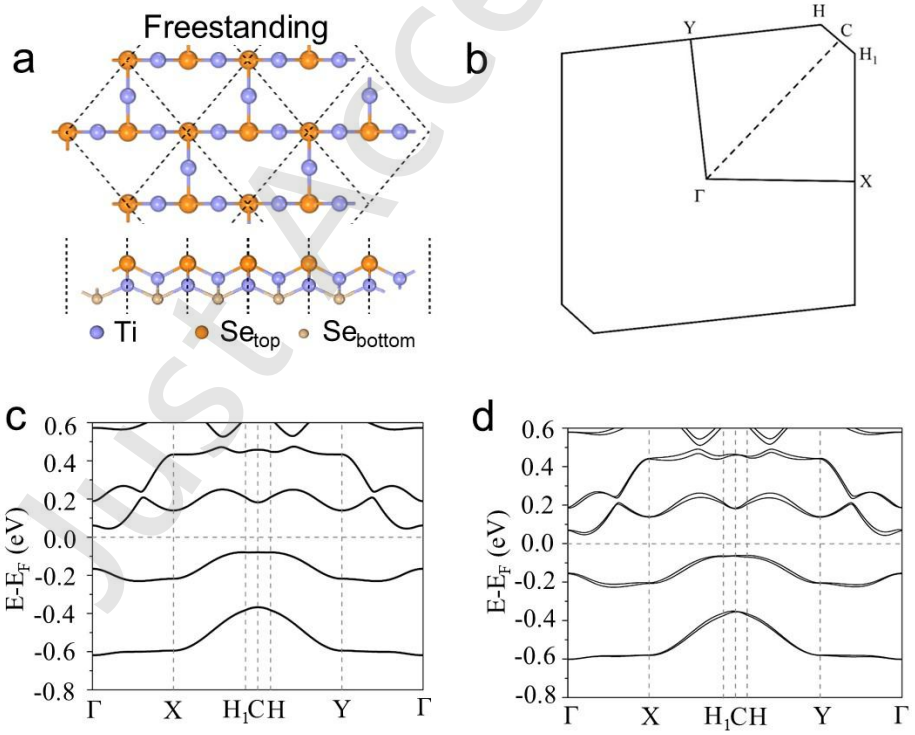

Figure 4. Calculated band structures of the freestanding Ti_3Se_4. (a) The atomic model of freestanding Ti_3Se_4. In the top panel, the bottom Se atoms are not shown. (b) Brillouin zone of monolayer Ti_3Se_4. (c, d) Calculated band structures of the freestanding Ti_3Se_4 without and with spin-orbit coupling (SOC), respectively.

We next investigated the thermal stability and the corresponding electronic structures of the fully relaxed free-standing Ti_3Se_4 monolayer. The freestanding Ti_3Se_4 is found to be stable and exhibits only minor structural differences compared to the monolayer derived from the Ti_3Se_4/Cu(111) interface, as shown in Fig. 4(a). Specifically, a set of Se atoms shift inward, forming a concave "brick" structure, while all Ti atoms shift upwards with the Ti atoms on the long side of the brick shifting further. These in-plane structural changes lead to lattice constants a= 5.87 Å, b= 5.87 Å, and θ= 99.8°. Figure 4(b) depicts the Brillouin zone of monolayer Ti_3Se_4. Figure 4(c) shows the calculated band structure of freestanding monolayer Ti_3Se_4 without SOC, revealing spin degenerate bands and a clear gap around the Fermi level. This band structure feature indicates that the freestanding Ti_3Se_4 monolayer is a semiconductor with a sizable band gap (~0.14 eV). Including SOC results in a slight band splitting, enlarging the band gap from 0.14 eV to 0.15 eV, as shown in Fig. 4(d). This small band gap suggests potential applications of this material in mid-infrared electronic devices.

4 Discussion

The QAH effect has vast potential for applications in quantum computing and advanced electronic devices. However, its practical use is hindered by the limited number of materials that exhibit the QAH effect, their instability in atmospheric conditions, and the need for ultra-low operational temperatures. Our computational findings offer a promising solution. We have shown that the presence of the substrate lifts the out-of-plane inversion symmetry, accompanied by minor lattice and structural adjustments, in the semiconducting Ti_3Se_4 monolayer, which can induce the QAH effect. This discovery suggests that similar modifications could be applied to air-stable 2D materials. In other words, the QAH effect could potentially be induced by slightly altering the atomic structure, which could be utilized either by applying mechanical stress (stretching, compressing, or bending) or temperature-induced structural phase transitions. Although these methods may not always achieve the QAH effect, they present a more efficient and practical approach compared to synthesizing new materials. Based on this example, we can further perform lattice tuning on other stable 2D semiconductor materials to investigate whether the QAH effect can emerge. We believe that sustained research and development in this direction can overcome existing limitations

and significantly promote future applications of the QAH effect.

6 Conclusions

In summary, we have successfully grown the Ti_3Se_4 monolayer on the Cu(111) substrate using the MBE method. The LEED analysis indicates that this monolayer has a $\sqrt{7} \times \sqrt{7}$ rhombus structure relative to the substrate. Our STM characterizations revealed a brick-like morphology. The structure of Ti_3Se_4 is further confirmed by DFT calculations and XPS characterizations. Our DFT calculations also indicate that the freestanding Ti_3Se_4 monolayer is a conventional semiconductor. However, when constrained, the monolayer exhibits a split in the original spin degeneracy, which has the potential to host the QAH effect. This significant change in properties results from slight shifts in atomic positions, making it feasible for experimental utilization. This work paves the way for using stable, well-known 2D materials to induce more intriguing electronic properties that are difficult to achieve in these materials.

Acknowledgements

We acknowledge financial support from the National Key R&D Program of China (Grants Nos. 2019YFA0308500 and 2018YFA0305800), the National Natural Science Foundation of China (Grants Nos. 61925111, 61888102, 11974422 and U23A6015), CAS Project for Young Scientists in Basic Research (YSBR-003) , the Strategic Priority Research Program of Chinese Academy of Sciences (Grants No. XDB28000000 and No. XDB30000000), the Fundamental Research Funds for the Central Universities, the Research Funds of Renmin University of China [No. 22XNKJ30 (W.J.)], and the CAS Key Laboratory of Vacuum Physics. Calculations were performed at the Physics Lab of High-Performance Computing of Renmin University of China, Shanghai Supercomputer Center and Beijing Supercomputing Center.

Electronic Supplementary Material: The structure characterization of CuSe ; The

measurement of the thickness of monolayer Ti_3Se_4 on Cu(111) ; STM images of monolayer Ti_3Se_4 under different biases ; Non-contact atomic force microscope image of monolayer Ti_3Se_4 ; XPS characterization of Ti_3Se_4

References

(1) Hasan, M. Z.; Kane, C. L. Colloquium: Topological insulators. *Rev. Mod. Phys.* **2010**, *82* (4), 3045-3067.

(2) Xu, Y.; Yan, B. H.; Zhang, H. J.; Wang, J.; Xu, G.; Tang, P. Z.; Duan, W. H.; Zhang, S. C. Large-Gap quantum spin Hall insulators in tin films. *Phys. Rev. Lett.* **2013**, *111* (13), 136804.

(3) Wang, C.; Zhu, X.; Nilsson, L.; Wen, J.; Wang, G.; Shan, X.; Zhang, Q.; Zhang, S.; Jia, J.; Xue, Q. In situ Raman spectroscopy of topological insulator Bi_2Te_3films with varying thickness. *Nano Res.* **2013**, *6* (9), 688-692.

(4) Yu, R.; Zhang, W.; Zhang, H.-J.; Zhang, S.-C.; Dai, X.; Fang, Z. Quantized Anomalous Hall Effect in Magnetic Topological Insulators. *Science* **2010**, *329* (5987), 61-64.

(5) Fu, L.; Kane, C. L. Topological insulators with inversion symmetry. *Phys. Rev. B* **2007**, *76* (4), 045302.

(6) Ren, Z.; Taskin, A. A.; Sasaki, S.; Segawa, K.; Ando, Y. Large bulk resistivity and surface quantum oscillations in the topological insulator Bi_2Te_2Se. *Phys. Rev. B* **2010**, *82* (24), 241306.

(7) Wang, J.; Li, H.; Chang, C.; He, K.; Lee, J. S.; Lu, H.; Sun, Y.; Ma, X.; Samarth, N.; Shen, S.; Xue, Q.; Xie, M.; Chan, M. H. W. Anomalous anisotropic magnetoresistance in

topological insulator films. *Nano Res.* **2012**, *5* (10), 739-746.

(8) Chang, C.-Z.; Zhang, J.; Feng, X.; Shen, J.; Zhang, Z.; Guo, M.; Li, K.; Ou, Y.; Wei, P.; Wang, L.-L.; Ji, Z.-Q.; Feng, Y.; Ji, S.; Chen, X.; Jia, J.; Dai, X.; Fang, Z.; Zhang, S.-C.; He, K.; Wang, Y.; Lu, L.; Ma, X.-C.; Xue, Q.-K. Experimental observation of the quantum anomalous Hall effect in a magnetic topological insulator. *Science* **2013**, *340* (6129), 167-170.

(9) Chen, Y. L.; Chu, J. H.; Analytis, J. G.; Liu, Z. K.; Igarashi, K.; Kuo, H. H.; Qi, X. L.; Mo, S. K.; Moore, R. G.; Lu, D. H.; Hashimoto, M.; Sasagawa, T.; Zhang, S. C.; Fisher, I. R.; Hussain, Z.; Shen, Z. X. Massive Dirac Fermion on the Surface of a Magnetically Doped Topological Insulator. *Science* **2010**, *329* (5992), 659-662.

(10) Qi, X. L.; Hughes, T. L.; Zhang, S. C. Topological field theory of time-reversal invariant insulators. *Phys. Rev. B* **2008**, *78* (19), 195424.

(11) Deng, Y.; Yu, Y.; Shi, M. Z.; Guo, Z.; Xu, Z.; Wang, J.; Chen, X. H.; Zhang, Y. Quantum anomalous Hall effect in intrinsic magnetic topological insulator $MnBi_2Te_4$. *Science* **2020**, *367* (6480), 895-900.

(12) Liu, C.-X.; Qi, X.-L.; Dai, X.; Fang, Z.; Zhang, S.-C. Quantum anomalous Hall effect in $Hg_{1-y}Mn_yTe$ quantum wells. *Phys. Rev. Lett.* **2008**, *101* (14), 146802.

(13) Yue, C.; Xu, Y.; Song, Z.; Weng, H.; Lu, Y.-M.; Fang, C.; Dai, X. Symmetry-enforced chiral hinge states and surface quantum anomalous Hall effect in the magnetic axion insulator $Bi_{2-x}Sm_xSe_3$. *Nat. Phys.* **2019**, *15* (6), 577–581.

(14) Checkelsky, J. G.; Yoshimi, R.; Tsukazaki, A.; Takahashi, K. S.; Kozuka, Y.; Falson, J.; Kawasaki, M.; Tokura, Y. Trajectory of the anomalous Hall effect towards the quantized

state in a ferromagnetic topological insulator. *Nat. Phys.* **2014**, *10* (10), 731-736.

(15) Chang, C.-Z.; Zhao, W.; Kim, D. Y.; Zhang, H.; Assaf, B. A.; Heiman, D.; Zhang, S.-C.; Liu, C.; Chan, M. H. W.; Moodera, J. S. High-precision realization of robust quantum anomalous Hall state in a hard ferromagnetic topological insulator. *Nat. Mater.* **2015**, *14* (5), 473-477.

(16) Wang, J.; Lian, B.; Zhang, H.; Xu, Y.; Zhang, S.-C. Quantum anomalous Hall effect with higher plateaus. *Phys. Rev. Lett.* **2013**, *111* (13), 136801.

(17) Xiao, D.; Jiang, J.; Shin, J.-H.; Wang, W.; Wang, F.; Zhao, Y.-F.; Liu, C.; Wu, W.; Chan, M. H. W.; Samarth, N.; Chang, C.-Z. Realization of the axion insulator state in quantum anomalous Hall sandwich heterostructures. *Phys. Rev. Lett.* **2018**, *120* (5), 056801.

(18) Liu, W.; West, D.; He, L.; Xu, Y.; Liu, J.; Wang, K.; Wang, Y.; van der Laan, G.; Zhang, R.; Zhang, S.; Wang, K. L. Atomic-scale magnetism of Cr-doped Bi_2Se_3 thin film topological insulators. *Acs Nano* **2015**, *9* (10), 10237-10243.

(19) Nan, J.; Liu, Y.; Chao, D.; Fang, Y.; Dong, S. Crystal defect engineering of Bi_2Te_3 nanosheets by Ce doping for efficient electrocatalytic nitrogen reduction. *Nano Res.* **2023**, *16* (5), 6544-6551.

(20) Geisenhof, F. R.; Winterer, F.; Seiler, A. M.; Lenz, J.; Xu, T.; Zhang, F.; Weitz, R. T. Quantum anomalous Hall octet driven by orbital magnetism in bilayer graphene. *Nature* **2021**, *598* (7879), 53-58.

(21) Serlin, M.; Tschirhart, C. L.; Polshyn, H.; Zhang, Y.; Zhu, J.; Watanabe, K.; Taniguchi, T.; Balents, L.; Young, A. F. Intrinsic quantized anomalous Hall effect in a moire heterostructure. *Science* **2020**, *367* (6480), 900-903.

(22) Polshyn, H.; Zhu, J.; Kumar, M. A.; Zhang, Y.; Yang, F.; Tschirhart, C. L.; Serlin, M.; Watanabe, K.; Taniguchi, T.; MacDonald, A. H.; Young, A. F. Electrical switching of magnetic order in an orbital Chern insulator. *Nature* **2020**, *588* (7836), 66-70.

(23) Chen, G.; Sharpe, A. L.; Fox, E. J.; Zhang, Y.-H.; Wang, S.; Jiang, L.; Lyu, B.; Li, H.; Watanabe, K.; Taniguchi, T.; Shi, Z.; Senthil, T.; Goldhaber-Gordon, D.; Zhang, Y.; Wang, F. Tunable correlated Chern insulator and ferromagnetism in a moire superlattice. *Nature* **2020**, *579* (7797), 56-61.

(24) Li, T.; Jiang, S.; Shen, B.; Zhang, Y.; Li, L.; Tao, Z.; Devakul, T.; Watanabe, K.; Taniguchi, T.; Fu, L.; Shan, J.; Mak, K. F. Quantum anomalous Hall effect from intertwined moire bands. *Nature* **2021**, *600* (7890), 641–646.

(25) Blochl, P. E. Projector augmented-wave method. *Phys. Rev. B* **1994**, *50* (24), 17953-17979.

(26) Kresse, G.; Joubert, D. From ultrasoft pseudopotentials to the projector augmented-wave method. *Phys. Rev. B* **1999**, *59* (3), 1758-1775.

(27) Kresse, G.; Furthmuller, J. Efficient iterative schemes for ab initio total-energy calculations using a plane-wave basis set. *Phys. Rev. B* **1996**, *54* (16), 11169-11186.

(28) Kresse, G.; Furthmuller, J. Efficiency of ab-initio total energy calculations for metals and semiconductors using a plane-wave basis set. *Comp. Mater. Sci.* **1996**, *6* (1), 15-50.

(29) Klimes, J.; Bowler, D. R.; Michaelides, A. Chemical accuracy for the van der Waals density functional. *J. Phys. Condens.* **2010**, *22* (2), 022201.

(30) Dion, M.; Rydberg, H.; Schröder, E.; Langreth, D. C.; Lundqvist, B. I. Van der Waals density functional for general geometries *Phys. Rev. Lett.* **2004**, *92* (24), 246401.

(31) Klimes, J.; Bowler, D. R.; Michaelides, A. Van der Waals density functionals applied to solids. *Phys. Rev. B* **2011**, *83* (19), 195131.

(32) Gao, L.; Sun, J.-T.; Lu, J.-C.; Li, H.; Qian, K.; Zhang, S.; Zhang, Y.-Y.; Qian, T.; Ding, H.; Lin, X.; Du, S.; Gao, H.-J. Epitaxial Growth of Honeycomb Monolayer CuSe with Dirac Nodal Line Fermions. *Adv. Mater.* **2018**, *30* (16), 1707055.

(33) Shkvarin, A. S.; Yarmoshenko, Y. M.; Yablonskikh, M. V.; Merentsov, A. I.; Shkvarina, E. G.; Titov, A. A.; Zhukov, Y. M.; Titov, A. N. The electronic structure formation of Cu_xTiSe_2 in a wide range (0.04 <x< 0.8) of copper concentration. *J. Chem. Phys.* **2016**, *144* (7), 074702.

(34) Song, Z.; Yi, J.; Qi, J.; Zheng, Q.; Zhu, Z.; Tao, L.; Cao, Y.; Li, Y.; Gao, Z.; Zhang, R.; Huang, L.; Li, G.; Xu, Z.; Wu, X.; Wang, Y.; Shen, C.; Zhang, Y.-Y.; Lu, H.; Lin, X.; Du, S.; Gao, H.-J. Line defects in monolayer $TiSe_2$ with adsorption of Pt atoms potentially enable excellent catalytic activity. *Nano Res.* **2022**, *15* (5), 4687-4692.

(35) Moulder, J. F.; Stickle, W. F.; Sobol, P. E.; Bomben, K. D.; Chastian, Eden Prairie, MN, USA. X-ray photoelectron spectroscopy. **1992**.

Electronic Supplementary Material

Exploring potential for semiconductor to quantum anomalous Hall insulator transitions via substrate-induced structural modifications in Ti_3Se_4 monolayers

Zhipeng Song[1,§], Haixia Cheng[2,6,§], Yun Cao[1], Qi Zheng[1], Yurou Guan[2], Chen Liu[3], Jierui Huang[1], Li Huang[1], Jiaou Wang[3], Hui Guo[1], Guangchao Chen[1], Chengmin Shen[1], Shixuan Du[1,4,5], Hongliang Lu[1,5] (✉), Wei Ji[2] (✉), Xiao Lin[1,5](✉) and Hong-Jun Gao[1,4,5]

[1]*University of Chinese Academy of Sciences and Institute of Physics, Chinese Academy of Sciences, Beijing 100190, China*

[2]*Beijing Key Laboratory of Optoelectronic Functional Materials & Micro-Nano Devices, Department of Physics, Renmin University of China, Beijing 100872, China*

[3]*Institute of High Energy Physics, Chinese Academy of Sciences, Beijing 100049, China*

[4]*Songshan Lake Materials Laboratory, Dongguan, Guangdong 523808, China*

[5]*CAS Center for Excellence in Topological Quantum Computation, University of Chinese Academy of Sciences, Beijing 100190, China*

[6]*Material Digital R&D Center, China Iron & Steel Research Institute Group, Beijing 100081, China*

Address correspondence to Hongliang Lu, luhl@ucas.ac.cn; Wei Ji, wji@ruc.edu.cn; Xiao Lin, xlin@ucas.ac.cn

Supporting information to https://doi.org/10.26599/NR.2025.94907123

S1. The structure of pore-free monolayer CuSe

To prepare monolayer Ti_3Se_4, we first construct a monolayer pore-free CuSe on the Cu(111) surface to establish a fixed amount of Se. Pore-free CuSe is a different structure compared to porous CuSe, which forms when a slightly higher amount of Se is deposited on the Cu(111) substrate.[1, 2] The pore-free monolayer CuSe has a hexagonal structure, as shown in Figure

S1(a), and its surface features striped moiré structures, as illustrated in Figure S1(b). This structure is not highly stable; when Ti is deposited on it (without further Se deposition), controlling the amount of Ti allows for the formation of monolayer Ti_3Se_4. In contrast, the CuSe with holes, which has higher structural stability, does not yield monolayer Ti_3Se_4 when Ti is deposited.

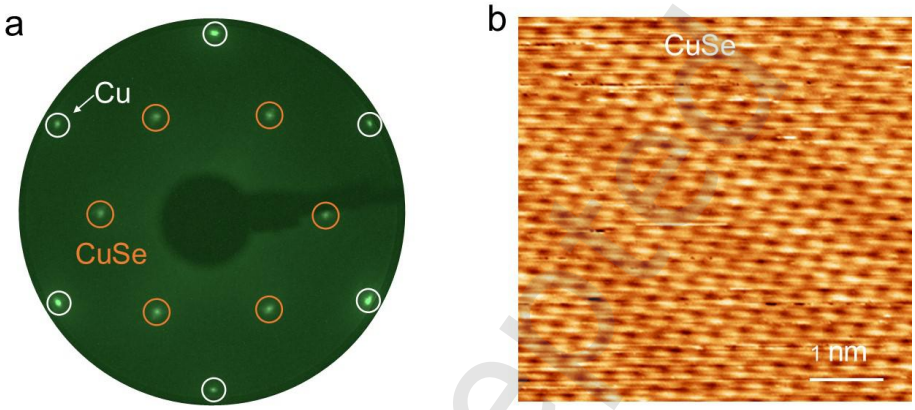

Figure S1. The structure characterization of CuSe. (a) LEED pattern showing diffraction spots from Cu(111) substrate (white circles) and monolayer CuSe (orange circles). The electron beam energy is 66 eV. (b) Atomically-resolved STM image of monolayer CuSe. The scanning parameters are V_S = -0.8 V, I_t = 0.5 nA, T=300 K.

S2. STM image of the boundary of a monolayer Ti_3Se_4

To determine the thickness of the monolayer Ti_3Se_4, we characterized its boundary and obtained morphological images and height data. On the left part of the image, we observed clusters, primarily consisting of Ti atoms. These clusters formed because there were insufficient Se atoms in the area to react with the Ti atoms, preventing the formation of a complete film.

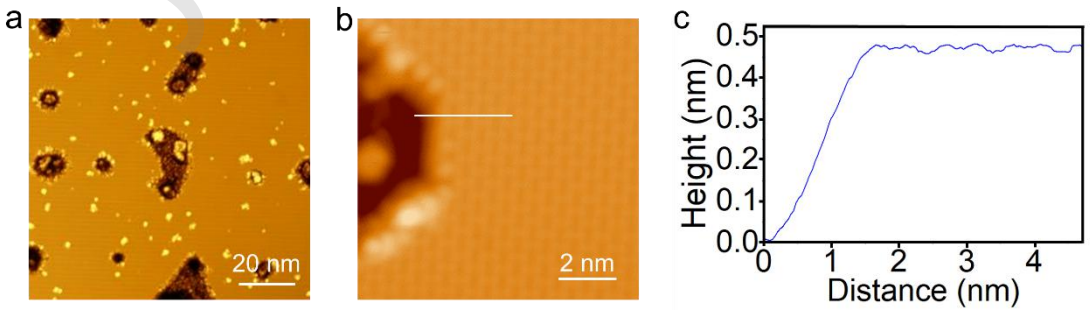

Figure S2. The measurement of the thickness of monolayer Ti_3Se_4 on Cu(111). (a) Large-scale STM image of monolayer Ti_3Se_4 (V_S = -0.8 V, I_t = 10 pA, T=4.5 k). (b) STM image of monolayer Ti_3Se_4 on Cu(111) showing an edge (V_S = -0.8 V, I_t = 10 pA, T=4.5 k). (c) Line profile taken along

the white line in (a), showing the height of monolayer Ti_3Se_4.

S3. STM morphology changes of monolayer Ti_3Se_4

STM offers unparalleled insights into the surface structures of materials by mapping the spatial distribution of electronic states. The morphology of these structures, however, can vary significantly with changes in the experimental conditions, such as the applied bias voltage. As with the monolayer Ti_3Se_4 samples we prepared, the surface morphology underwent significant changes with the variation of the bias voltage, transitioning from brick-like to rectangular morphologies under specific voltage conditions, as shown in Figure S3.

The observed changes in morphology can be attributed to the alterations in the local electronic structure caused by varying the bias voltage. When a higher bias voltage is applied, it may involve more electronic states in surface Se atoms, which can cause greater overlap of electron wavefunctions in certain areas, giving a brick-like morphology. Conversely, lower bias voltages might make lower energy electronic states more apparent, potentially resulting in a more dispersed electron cloud that manifests as a rectangular surface morphology. The result adds to the existing literature by documenting a rare observation of morphological transitions between rectangular and brick-like structures, contributing to the broader knowledge of surface science.

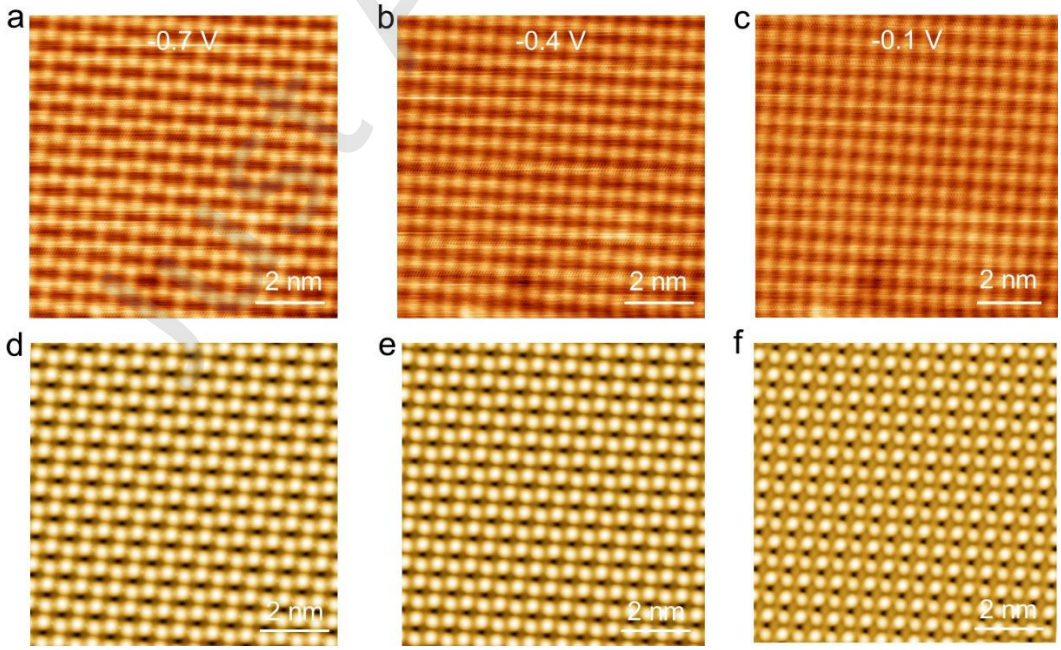

Figure S3. STM images of monolayer Ti_3Se_4 under different biases. (a, b, c) High-resolution STM image of monolayer Ti_3Se_4 at -0.7 V, -0.4 V and -0.1 V, respectively. The tunneling current is 50 pA. STM image shows a brick-like morphology when the absolute value of bias (|V|) > 0.4 V and the rectangle morphology when |V|<0.4 V. (d, e, f) STM simulation of monolayer Ti_3Se_4 on

Cu(111) substrate at -0.7 V, -0.4 V and -0.1 V, respectively. The simulated STM images are consistent with the experiments under different biases.

S4. AFM morphology of monolayer Ti_3Se_4

Unlike STM, which operates based on electron tunneling, atomic force microscopy (AFM) works on a different principle. It creates a map of the surface morphology by measuring the force between the probe and the sample, instead of electron tunneling. This approach is especially useful for materials like monolayer Ti_3Se_4, where the actual surface morphology could be masked in STM images due to the effects of electronic states under different bias voltages. Using AFM allows for greater atomic resolution of the surface, emphasizing characteristics that are not influenced by electronic effects. As demonstrated in Figure S4, the brick-like morphology obtained with AFM represents the intrinsic structure of monolayer Ti_3Se_4.

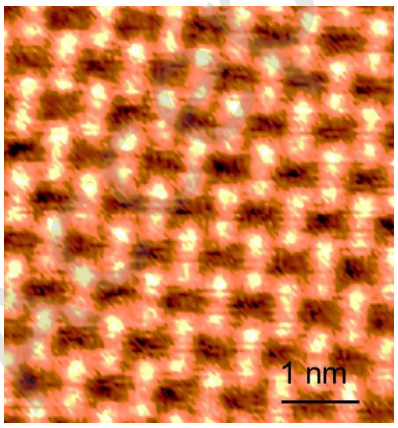

Figure S4. Non-contact atomic force microscope image of monolayer Ti_3Se_4, revealing the real surface atomic structure. AFM scanning parameters: amplitude=200 pm.

S5. XPS characterization of monolayer Ti_3Se_4

The initial synthesis of a new monolayer 2D material necessitates the determination of its structure and composition. For our newly synthesized monolayer Ti_3Se_4, we have characterized the crystal structure and surface morphology using LEED and STM, respectively, and have simulated its structural features using DFT calculations. Nonetheless, the valence states of the compound require further experimental investigation through XPS to identify the valence states of its constituent elements and to acquire a detailed understanding of the material's electronic structure. Comprehensive characterization of this new 2D material and verification of its composition are essential to enhance our understanding of its potential applications.

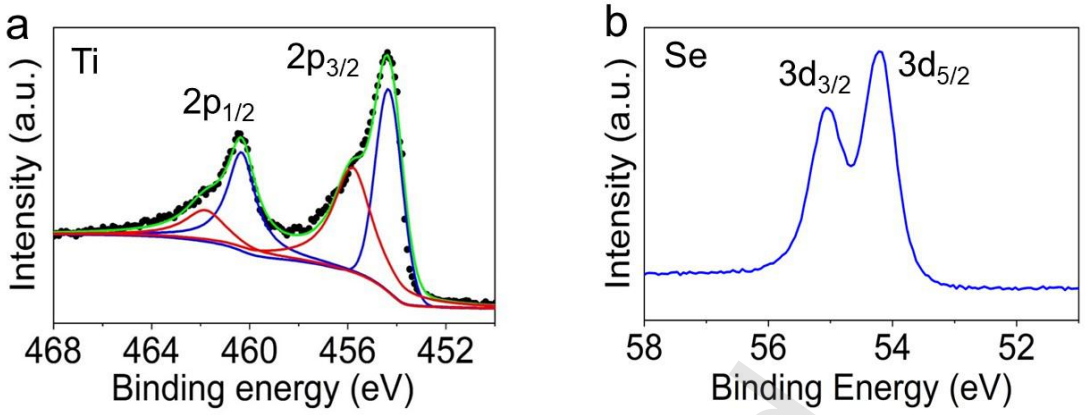

Figure S5. XPS characterization of Ti_3Se_4. (a) XPS measurements for the binding energies of Ti 2p electrons. The blue and red curves are obtained by peak separation method, corresponding to the Ti^{2+} and Ti^{3+} valence states of Ti ions in Ti_3Se_4, respectively. Discrete black points represent the raw data and the green curve is the fitting curve. (b) XPS spectrum of the Se 3d core levels, revealing the chemical state of Se^{2-}.

(1) Lin, X.; Lu, J. C.; Shao, Y.; Zhang, Y. Y.; Wu, X.; Pan, J. B.; Gao, L.; Zhu, S. Y.; Qian, K.; Zhang, Y. F.; Bao, D. L.; Li, L. F.; Wang, Y. Q.; Liu, Z. L.; Sun, J. T.; Lei, T.; Liu, C.; Wang, J. O.; Ibrahim, K.; Leonard, D. N.; Zhou, W.; Guo, H. M.; Wang, Y. L.; Du, S. X.; Pantelides, S. T.; Gao, H. J. Intrinsically patterned two-dimensional materials for selective adsorption of molecules and nanoclusters. *Nat. Mater.* **2017**, *16* (7), 717-721.

(2) Song, Z.; Huang, J.; Zhang, S.; Cao, Y.; Liu, C.; Zhang, R.; Zheng, Q.; Cao, L.; Huang, L.; Wang, J.; Qian, T.; Ding, H.; Zhou, W.; Zhang, Y.-Y.; Lu, H.; Shen, C.; Lin, X.; Du, S.; Gao, H.-J. Observation of an Incommensurate Charge Density Wave in Monolayer $TiSe_2$/CuSe/Cu(111) Heterostructure. *Phys. Rev. Lett.* **2022**, *128* (2), 026401.